Host-guest Chemistry Meets Electrocatalysis: Cucurbit[6]uril on a Au Surface as Hybrid System in CO_2 Reduction

Andreas Wagner,[a,1] Khoa H. Ly,[a,1,2] Nina Heidary,[a,3] István Szabó,[b] Tamás Földes,[b] Khaleel I. Assaf,[c] Steven J. Barrow,[d,4] Kamil Sokołowski,[d,e] Mohamed Al-Hada,[f] Nikolay Kornienko,[a,3] Moritz F. Kuehnel,[a,5] Edina Rosta,[b] Ingo Zebger,[g] Werner M. Nau,[c] Oren A. Scherman,[d,*] Erwin Reisner [a,*]

[a] Christian Doppler Laboratory for Sustainable SynGas Chemistry, Department of Chemistry, University of Cambridge, Lensfield Road, Cambridge CB2 1EW, United Kingdom

[b] Department of Chemistry, King's College London, 7 Trinity Street, SE1 1DB, London, United Kingdom

[c] Department of Life Sciences and Chemistry, Jacobs University Bremen, Campus Ring 1, 28759 Bremen, Germany

[d] Melville Laboratory for Polymer Synthesis, Department of Chemistry, University of Cambridge, Lensfield Road, Cambridge CB2 1EW, United Kingdom

[e] Institute of Physical Chemistry, Polish Academy of Sciences, Kasprzaka 44/52, 01-224 Warsaw, Poland

[f] Cavendish Laboratory, Department of Physics, University of Cambridge, JJ Thomson Ave, Cambridge CB3 0HE, United Kingdom

[g] Max Volmer Laboratorium für Biophysikalische Chemie, Sekr. PC14, Institut für Chemie, Technische Universität Berlin, Straße des 17. Juni 135, 10623 Berlin, Germany

[1] Contributed equally to this work.

[2] Present address: Fakultät für Chemie und Lebensmittelchemie, Technische Universität Dresden, 01062 Dresden, Germany

[3] Present address: Department of Chemistry, Université de Montréal, Roger-Gaudry Building, Montreal, Quebec, H3C 3J7, Canada

[4] Present address: School of Applied Chemistry and Environmental Science, RMIT University, Melbourne, 3000, Victoria, Australia

[5] Present address: Department of Chemistry, Swansea University, College of Science, Singleton Park, Swansea SA2 8PP, U.K.

[*] To whom correspondence should be addressed: reisner@ch.cam.ac.uk, oas23@cam.ac.uk

Abstract

The rational control of forming and stabilizing reaction intermediates to guide specific reaction pathways remains a major challenge in electrocatalysis. In this work, we report a surface active site engineering approach for modulating electrocatalytic CO_2 reduction using the macrocycle cucurbit[6]uril (CB[6]). A pristine gold surface functionalized with CB[6] nanocavities was studied as a hybrid organic-inorganic model system that utilizes host-guest chemistry to influence the heterogeneous electrocatalytic reaction. The combination of surface-enhanced infrared absorption (SEIRA) spectroscopy and electrocatalytic experiments in conjunction with theoretical calculations support capture and reduction of CO_2 inside the hydrophobic cavity of CB[6] on the gold surface in aqueous $KHCO_3$ at negative potentials. SEIRA spectroscopic experiments show that the decoration of gold with the supramolecular host CB[6] leads to an increased local CO_2 concentration close to the gold interface. Electrocatalytic CO_2 reduction on a CB[6]-coated gold electrode indicates differences in the specific interactions between CO_2 reduction intermediates within and outside the CB[6] molecular cavity, illustrated by a decrease in CO current density, but almost invariant H_2 production compared to unfunctionalized Au. The presented methodology and mechanistic insight will guide future design of molecularly engineered catalytic environments through interfacial host-guest chemistry.

Introduction

The electrocatalytic reduction of CO_2 using renewable energy sources offers an attractive route to produce storable carbon-neutral fuels.[1,2] For this technology to become commercially viable, catalysts that promote the challenging multi electron/proton transfer reaction at minimal energy-penalty, a high rate and selectivity need to be developed. Currently, CO_2 reduction suffers from significant overpotentials, sluggish kinetics and control of selectivity as well as the low solubility of CO_2 in aqueous electrolytes.[3–5] Gold (Au) is generally considered the most active electrocatalyst for CO generation with a catalytic onset potential *ca.* 300 mV more negative than the standard potential for CO_2 to CO reduction on flat electrodes.[6–8] The catalytic mechanism on Au is believed to involve a surface-bound COOH (*COOH) intermediate, which is subsequently further reduced by $1e^- / 1H^+$ transfer to yield CO (*CO) that is finally liberated from the surface. Theoretical predictions indicate that stronger binding of the *COOH intermediate relative to *CO may be needed for enhanced CO evolution activity.[9,10] However, the binding energies of *COOH and *CO on electrocatalysts generally correlate,[11] therefore stabilization of *COOH would simultaneously stabilize *CO and thus disfavor its required desorption. This scaling relationship impedes a straightforward approach to independently fine-tune surface properties for higher activities; limiting the development of low overpotential single-site metal catalysts.[12]

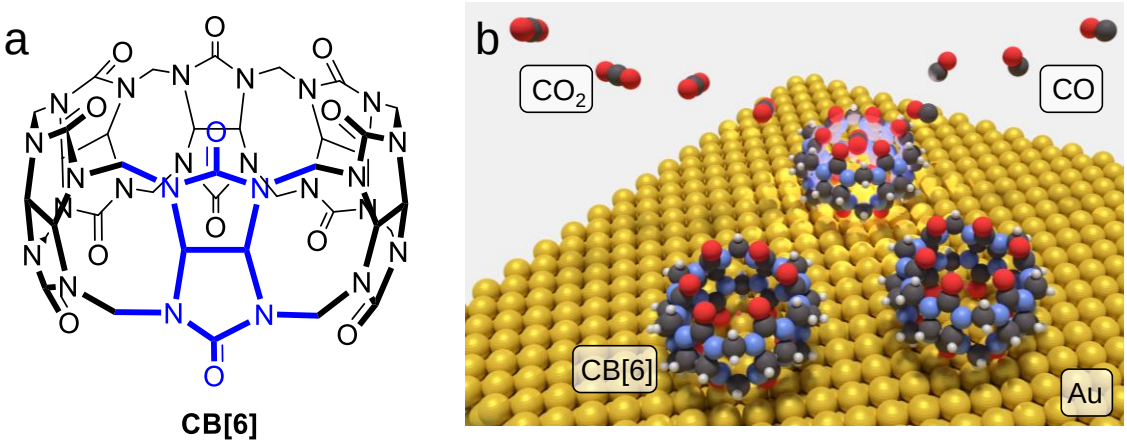

Fig. 1. (a) CB[6] structure with monomeric building block highlighted in blue. (b) Schematic illustration of CO_2 conversion to CO within the cavity of CB[6] adsorbed on Au surface.

To this end, different approaches such as alloying,[13,14] nano-structuring[15] and molecular surface modifications[16–20] have recently gained attention. Nevertheless, molecular engineering of an electrocatalytic surface site remains challenging. Nature, on the other hand, has developed very effective catalytic systems that surpass the limits of scaling relationships. Enzymes such as carbon monoxide dehydrogenase and formate dehydrogenase are able to reversibly interconvert CO_2 at the thermodynamic potential with quantitative product selectivity at their precious-metal free active sites.[21–23] While details about their reaction mechanisms are still under debate, a hydrophobic active site cavity as well as stabilization of intermediates by a highly specific second coordination sphere are believed to be crucial for their high activity as well as selectivity.[9,24,25]

In our efforts to create analogous synthetic reaction environments, we envision supramolecular host-guest chemistry as a powerful tool to modulate electrocatalytic reactions by selectively favoring certain species due to highly specific binding affinities. Cucurbit[*n*]urils (CB[*n*], where n = 5-8) are a class of promising host molecules for this purpose. These barrel-shaped organic macrocycles are water soluble and have found broad applications in materials chemistry, drug delivery systems, as well as sensing and catalysis (Fig. 1a).[26,27] CB[*n*]s are able to shift the reduction potential of electrochemical processes by selectively stabilizing certain species,[28,29] *e.g.* positively shifted half-wave potentials of ferrocene and methyl viologen upon complexation with CB[7] due to differential stabilization of the oxidized *vs.* reduced species within the cavity.

The cavities of CB[*n*] are highly hydrophobic[30] and bind a plethora of small organic guests (for $n \geq 6$) as well as gas molecules (for $n \leq 6$).[26] In aqueous solution, a large number of gases (*e.g.* CH_4, acetylene, cyclopentane) form inclusion complexes within CB[6].[31] Their negatively polarized carbonyl-lined portals exhibit high affinity towards metal surfaces allowing for facile supramolecular functionalization of electrodes.[32] In contrast, other hosts such as pillararenes, cyclodextrins and calixarenes typically rely on additional steps for electrode immobilization, which often afford increased distances between the host cavity and the surface.[33–35] Their ability to directly affect surface bound species is thereby diminished.

It has been shown spectroscopically and by gravimetric measurements that CB[6] can be used as a highly porous solid-state adsorbent for gaseous CO_2 with high selectivity

over CO, rendering this molecule attractive for combining host-guest chemistry and electrocatalytic CO_2 reduction studies.[36,37] However, to the best of our knowledge, neither CO_2 complexation within CB[6] in solution has been demonstrated, nor has CB[6] been used in electrocatalytic CO_2 reduction.

In this work, we study CB[6] as a prototypical synthetic organic cavity system for facile manipulation of the heterogeneous CO_2 reduction on Au, a well-studied model electrocatalyst (Fig. 1b). Firstly, the host-guest interaction of CO_2 with CB[6] is studied in homogeneous aqueous solutions both experimentally as well as computationally. Subsequently, we employ surface-enhanced infrared absorption (SEIRA) spectroscopy combined with electrochemistry to investigate the behavior of CO_2 within CB[6] on the Au surface during electrocatalysis.

Results and Discussion

Interaction of CO_2 with CB[6] in solution

The inclusion of CO_2 in CB[6] was monitored in aqueous $KHCO_3$ (0.1 M) using Fourier-transform infrared (FTIR) spectroscopy in transmission mode (Fig. 2a). The asymmetric stretching mode of $^{12}CO_2$ was found at 2343 cm^{-1}, in line with previously reported values for $^{12}CO_2$ in solution.[38] In the presence of 8.44 mM CB[6], an additional shoulder was detected at 2333 cm^{-1}. This band was exclusively observed in a $^{12}CO_2$-purged electrolyte solution (Fig. S1) and was therefore assigned to an interaction between CO_2 and CB[6] ('CB[6]•CO_2'). The corresponding $^{13}CO_2$ asymmetric stretching vibration[38] at 2278 cm^{-1} displayed an identical shift by 10 cm^{-1} to 2268 cm^{-1}, confirming this band to originate from CO_2.

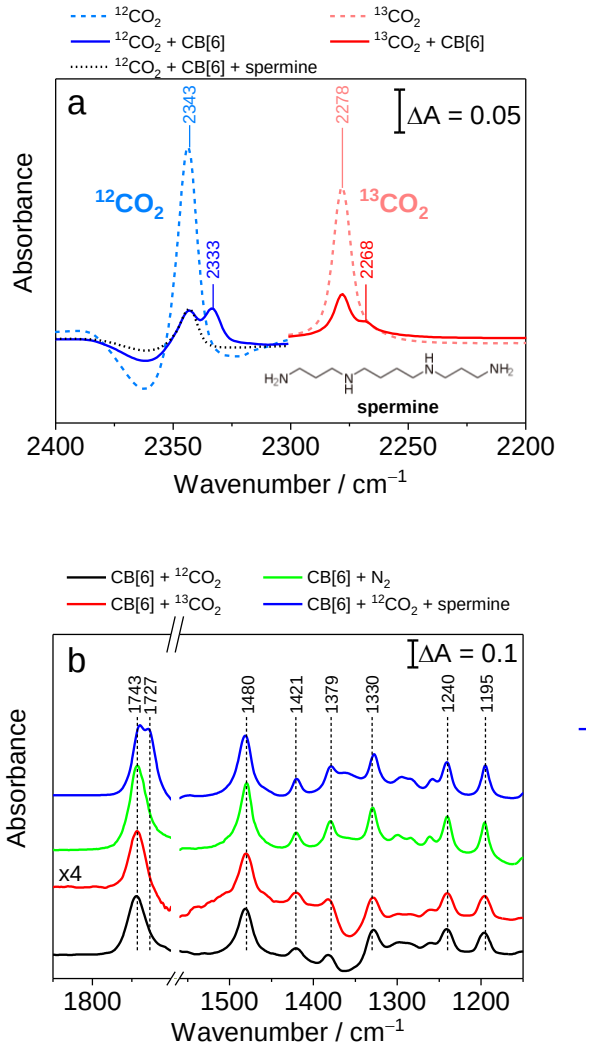

Fig. 2. FTIR spectra of CB[6] solutions recorded in transmission mode. (a) Absorbance spectra of asymmetric stretching modes of $^{12}CO_2$ in aqueous $KH^{12}CO_3$ (0.1M) and $^{13}CO_2$ in $NaH^{13}CO_3$ (0.1 M) solution. The reference spectra for dashed spectra were the N_2 purged electrolytes. Spectra of CB[6] from which the CB-free CO_2 reference spectrum was subtracted, display a shoulder at 2333 cm^{-1} and 2268 cm^{-1}, respectively. The addition of spermine (strong CB[6] cavity binder) leads to disappearance of the 2333 cm^{-1} band. The broad negative band at *ca.* 2360 cm^{-1} results from small atmospheric CO_2 variations between measurements. (b) IR spectra of region below 1800 cm^{-1} representing the vibrational modes for CB[6] in $^{12}CO_2$-purged 0.1 M $KH^{12}CO_3$, and $^{13}CO_2$-purged 0.1 M $NaH^{13}CO_3$ which exhibit no band shifts in comparison to the N_2-purged 0.1 M $KH^{12}CO_3$ solution. Addition of spermine leads to an

additional band at 1727 cm^{-1} assigned to carbonyl functional groups of CB[6], presumably occurring due to the interaction of the spermine nitrogen and the CB[6] carbonyl ring. Spectrum of CB[6] $^{13}CO_2$-purged sample was multiplied by a factor of 4 for better comparison (see experimental details, SI).

The observed shift matches the previously reported values for the asymmetric stretching mode of CO_2 confined in solid CB[6] at 2336 cm^{-1}. [36,37] Addition of spermine, a well-known CB[6] guest with a high binding affinity,[26] led to disappearance of the band at 2333 cm^{-1}, in line with a competitive displacement of CO_2 from the cavity. Moreover, the IR bands of the CB[6] framework remained unchanged in the presence of N_2 and $^{12}CO_2/^{13}CO_2$ indicating that the CB[6]•CO_2 (binding) interaction is weak and non-directional (Fig. 2b). In contrast, spermine addition gave rise to a strong additional band at 1727 cm^{-1}. This band can be rationalized by a shift of the carbonyl stretching mode from 1743 cm^{-1} by 16 cm^{-1} as a result of electrostatic interactions with the positively-charged amine functional group of spermine.[39] Analogously, the unaltered CB[6] carbonyl band in the presence of CO_2, when compared to CB[6]•spermine host-guest complex, suggests that CO_2 is not merely associated with the carbonyl portal region of CB[6]. The IR data strongly suggests that CO_2 is bound inside the CB[6] cavity in solution with an IR marker band located at 2333 cm^{-1}. We note that the binding of CO to CB[6] could not be probed due to its low solubility in the reaction solution.

The assignment of the CO_2 interaction with CB[6] is further corroborated by density functional theory (DFT) and molecular dynamics (MD) simulations (Table S1 and Fig. S2-5). Both methods show a stronger binding of CO_2 over CO in CB[6], in line with previously reported DFT results.[40] A free energy profile based on umbrella sampling MD simulations of CO_2 and CO is shown in Fig. 3a. The results suggest that CO_2 and CO need to overcome a low energy barrier when entering the cavity and reach an energy minimum at the cavity center. CO_2 was found to bind with two possible conformations in the pocket (second local minima found at $z = \pm 3.1$ Å). A snapshot of the final state after 22 ns of a MD simulation in $KHCO_3$ (0.1 M) is shown in Fig. 3b. The CO molecule was initially placed in the cavity center and was found to be eventually replaced by two CO_2

molecules at the given concentration. The free energy profiles were used to calculate the binding constants K_{a,CO_2} = 105 M^{-1} and $K_{a,CO}$ = 5 M^{-1} for CB[6]•CO_2 and CB[6]•CO, respectively (binding free energy of 6.4 and 4.1 kcal mol^{-1} respectively, see SI for computational details).

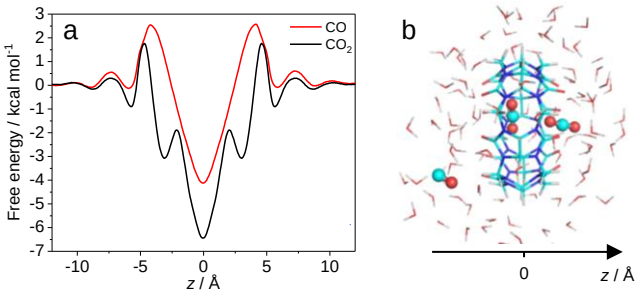

Fig. 3. CO_2 and CO inclusion in CB[6] in 0.1 M $KHCO_3$ studied by MD simulation. (a) Free energy profile of CO_2 and CO passing through the cavity of CB[6] along a central axis (*z*-axis is illustrated in b) based on umbrella sampling MD simulations. (b) Snapshot of MD simulation with one 'deep-cavity' bound CO_2, one CO_2 loosely associated with carbonyl ring and one unbound CO.

To quantify the binding of CO_2 and CB[6] experimentally, fluorescent dye displacement measurements were performed (Fig. 4a and Fig. S6). This technique utilizes the fluorescence of the host-guest complex of CB[6] with an indicator dye, such as *trans*-4[4-(dimethylamino)styryl]-1-methylpyridinium (DSMI, inset Fig. 4a). DSMI is weakly fluorescent on its own, but strongly fluorescent in its complexed state.[41] The competitive binding of CO_2 and DSMI to the CB[6] cavity (Fig. 4b) was used to determine a binding constant (K_{a,CO_2}) of 250 ± 100 M^{-1} in 0.1 M $KHCO_3$ for the CB[6]•CO_2 host-guest complex. The experimental finding was qualitatively confirmed with a second indicator dye (Fig. S6). This sizable affinity is in good agreement with the computational data. Unfortunately, CO, the CO_2 reduction product, owing to its low solubility, afforded only a small change in fluorescence (Fig. 4a), which prevented an accurate quantification of its binding constant. However, well-established trends of gas affinities and corresponding volume/packing coefficients[31] and the performed DFT and MD calculations suggest a much lower binding of CO than that of CO_2 to CB[6]. These findings indicate that there

is no product inhibition (*i.e.* CO occupying the CB[6] pocket due to higher binding affinity than CO_2), which is a general concern in (supramolecular) catalysis.[42]

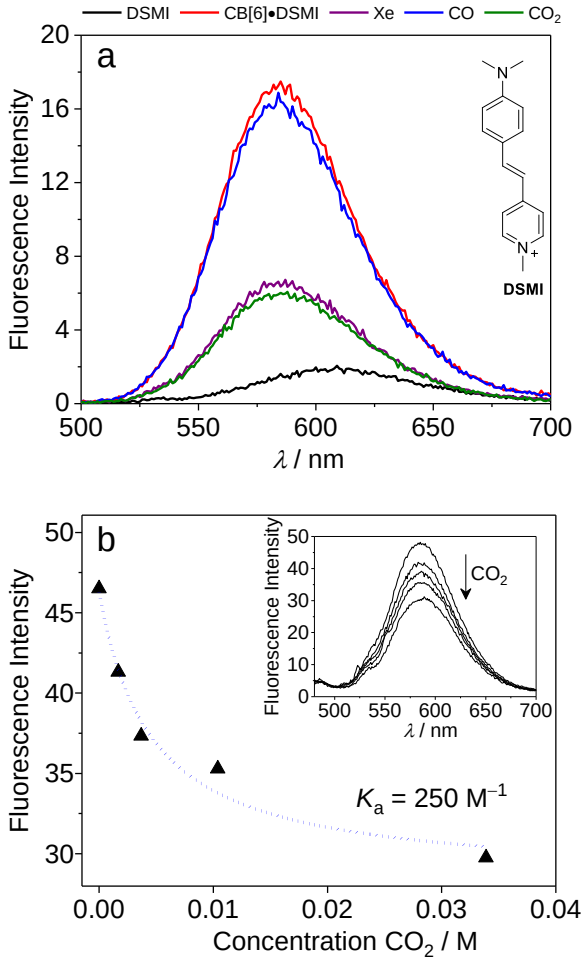

Fig. 4. Fluorescent dye displacement measurements. (a) Fluorescence intensity of CB-free DSMI, and the CB[6]•DSMI complex with and without competitive guests. The solution was saturated with the respective gas. Xe was used as a control with known binding affinity. The DSMI counterion (iodide) was removed for clarity. (b) Decrease in fluorescence of CB[6]•DSMI complex with increasing CO_2 concentration to calculate the binding affinity of CO_2•CB[6] based on the known binding affinity of DSMI. The concentration of CO_2 was determined via Henry's law (see SI for details). Experimental conditions: 0.1 M $KHCO_3$, [dye] = 1 μM, [CB[6]] = 50 μM, excitation wavelength = 283 nm, $K_{a,DSMI}$ determined as 2100 M^{-1} in 0.1 M $KHCO_3$ (Fig. S6).

Au electrode modification with CB[6]

The binding of CB[6] to Au surfaces has previously been reported,[32,43] but rarely quantitatively. The effect of the solvent as well as the nature and concentration of the electrolyte were suspected to have a large effect on the surface adsorption equilibrium. Solubility of CB[6] in water is typically very low (<100 µM),[44] but it can be readily increased by more than two orders of magnitude through addition of cationic species to the solution.[45] Besides the increased solubility, the interaction of cations with CB[6] influences the kinetics of host-guest complex formation.[46] As an additional complexity, cations themselves have been shown to effect CO_2 reduction on heterogeneous electrocatalysts.[47–50] Considering these multiple intricate effects of cations in the system, we employed an aqueous $KHCO_3$ (0.1 M) electrolyte solution, which is also commonly used in CO_2 reduction catalysis.[51,52] This concentration fulfils the necessity for supporting electrolytes during electrocatalytic CO_2 reduction and overcomes the limited solubility of CB[6] while minimizing the effects of cations on the host-guest complexation as well as on CO_2 reduction to a minimum. The adsorption of CB[6] on Au was first quantified by quartz-crystal microbalance (QCM) measurements at open circuit potential in N_2-purged $KHCO_3$ as shown in Fig. 5a. The coverage was estimated using the Sauerbrey model,[53] assuming a flat gold surface and a van-der-Waals radius of 'rigid' CB[6] of 14.4 Å.[45] A theoretical monolayer coverage of *ca.* (80 ± 20) % for 1.69 mM CB[6] was determined with a Langmuir isotherm. Considering the highest density of hexagonally-packed circles within a plane (*ca.* 90 %), the data obtained from QCM is close to an optimally covered surface.

QCM was not only applied to study surface adsorption processes by mass changes, but is also further utilized to obtain insights into the viscoelasticity of the adsorbed layer by studying its dissipation behaviour.[54] This can be particularly useful to gather information on changes of layer packing or, importantly, multilayer formation.[55,56] Measurements indicated that for concentrations > 0.8 mM the dissipation starts to increase, suggesting the formation of multilayers of CB[6] (Fig. S7). Multilayer build-up of CB[6] on surfaces has been observed previously for CB[6] in solutions containing Na^+.[57] Furthermore, formation of chain-like coordination polymers between CB[6] and K^+ has been reported in the solid state.[58,59]

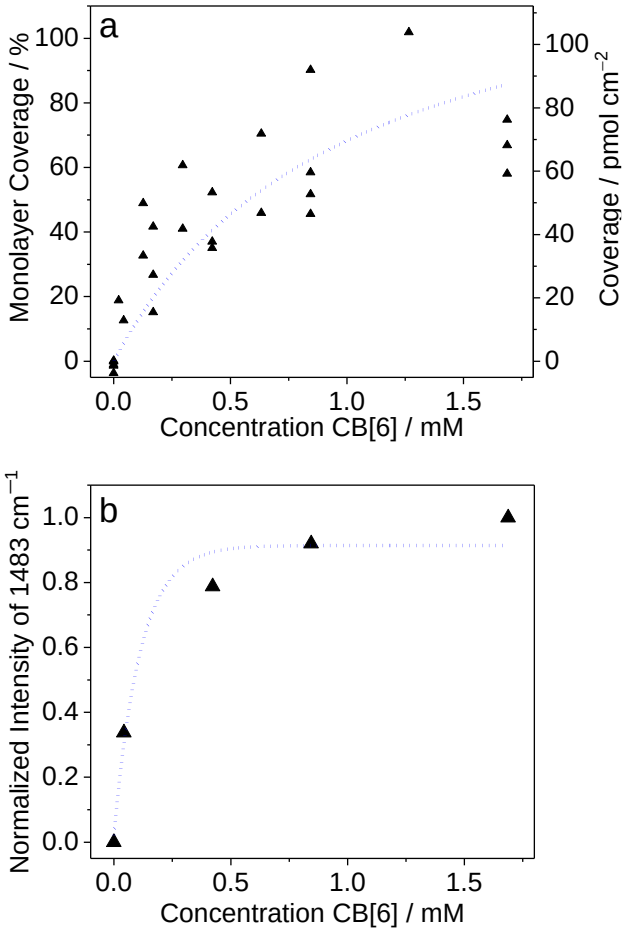

Fig. 5. Surface adsorption of CB[6] on Au. (a) Monolayer coverage of CB[6] on Au based on quartz-crystal microbalance measurements at open circuit potential. The data was modelled with the Sauerbrey equation and fitted with a Langmuir isotherm (blue dashed line). (b) Increase in relative intensity of CB[6] band at 1480 cm^{-1} band in SEIRA measurements and exponential fit to guide the eye (blue dashed line).

The interaction of CB[6] with the Au surface was further probed by SEIRA spectroscopy, which selectively monitors the Au-electrolyte interface (see below).[60,61] The vibrational band pattern of CB[6] revealed significantly different relative intensities between SEIRA and transmission measurements due to surface selection rules, indicating a preferential binding geometry of CB[6] on the surface compared to the isotropic case in solution (Fig. S8). A notable shift of the carbonyl stretching mode from 1743 cm^{-1} in

solution to 1737 cm^{-1} on the Au surface further suggests an interaction between (one of) the carbonyl-lined portals of CB[6] with the gold surface; in line with previous reports.[32,43,62] Fig. 5b shows the normalized intensity of the intense 1483 cm^{-1} marker band of CB[6] as a function of the CB[6] concentration in solution. No notable increase was observed for concentrations higher than *ca.* 1.3 mM (Fig. S9), matching the concentration at which multilayer formation was observed in QCM measurements (Fig. S7). As the SEIRA intensity I decreases significantly with distance d from the electrode surface ($I \sim d^{-6}$), potential multilayers of CB[6] cannot be monitored.[63] SEIRA as well as X-Ray photoelectron spectroscopy (XPS) indicated a stable surface-bound CB[6] layer after overnight soaking in CB[6]-free 0.1 M $KHCO_3$ aqueous electrolyte solution (Fig. S10-11).

SEIRA measurements of CB[6]•CO_2 under polarization

SEIRA spectroscopy has recently gained increased attention in the field of CO_2 reduction catalysis due to its high sensitivity for surface processes.[64–67] Typically, reported studies exploit the strong IR activity of CO and HCO_3^-/CO_3^{2-} and track specific bands to monitor product stability and binding, bicarbonate/CO_2 equilibrium, and the role of cations. In this study, we specifically focus on the role of CO_2 and its fate upon inclusion into CB[6] during electrocatalytic turnover (see Fig. 6).

Upon purging the electrolyte solution containing 1.69 mM CB[6] with CO_2, the band at 2333 cm^{-1} assigned to CB[6]•CO_2 appeared, indicating that CO_2 can efficiently penetrate the CB[6] cavity when the host molecule is bound to the Au surface. Compared to the isotropic case in solution, the CB[6]•CO_2 band showed an increased intensity in the SEIRA spectra (Fig. 6a) relative to the unaltered $CO_{2(aq)}$ band at 2343 cm^{-1}, suggesting an increase in the total CO_2 concentration (*i.e.* free $CO_{2(aq)}$ and CB[6]•CO_2) at the Au-electrolyte interface. We speculate that the binding of CB[6] to the Au surface together with its ability to host CO_2 acts as a driving force for CO_2 accumulation at the electrode surface.

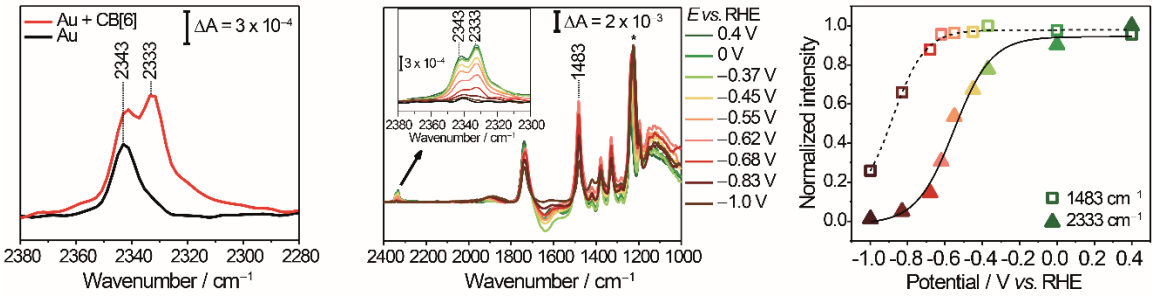

Fig. 6. SEIRA measurements of CB[6]•CO_2 on Au. (a) SEIRA spectra of CO_2 purged 0.1 M $KHCO_3$ (black) and 1.69 mM CB[6] in 0.1 M $KHCO_3$ (red). Reference spectra: Unmodified Au in Argon purged 0.1 M $KHCO_3$. (b) Potential dependent SEIRA spectra showing slow desorption of CB[6] from the surface at potentials more negative than –0.7 V *vs.* RHE, Inset: CB•CO_2 band at 2333 cm^{-1} decreases rapidly at CO_2 reduction turnover potentials. Reference spectra: Unmodified Au in Argon purged 0.1 M $KHCO_3$ at respective potentials. A spectral artefact (due to SiO_2 from the prism) at 1239 cm^{-1} marked with a star* was found to increase. (c) Normalized (between maxima and 0) intensity decline of band at 2333 cm^{-1} and 1483 cm^{-1} with sigmoidal fits. Conditions: 1.69 mM CB[6] in 0.1 M $KHCO_3$. All potentials were *iR* corrected (see SI for details).

SEIRA spectroscopic experiments in a three-electrode configuration were performed to investigate the behavior of the supramolecular complex on the surface at reductive potentials. To the best of our knowledge, the nature of the interaction, as well as the stability of CB[6] on Au under electrochemical polarization has not yet been assessed in the literature. SEIRA spectra recorded at various potentials revealed that CB[6] starts to reversibly desorb from the electrode at –0.7 V *vs.* reversible hydrogen electrode (RHE; Fig. 6). This is further confirmed by *ex situ* XPS measurements (Fig. S12). Note that the anchoring of the carbonyl-lined portal of CB[6] is significantly different to chemisorption through commonly employed thiol groups on Au that suffers from low electrochemical stability under reductive conditions.[68] Though several groups have recently reported that multi-dentate thiol-anchoring provides improved stability of co-catalysts for CO_2 reduction, reductive desorption effects were not discussed in detail.[18,19]

As shown in the inset in Fig. 6b-c, the intensity of the CB[6]•CO_2 band started to decline at potentials below *ca.* –0.4 V *vs.* RHE, matching the catalytic onset for CO_2

reduction (see below). This observation indicates the reduction of CO_2 inside the Au-immobilized CB[6] cavity. A mere desorption of CB[6] hosting CO_2 at very reducing conditions, which would also cause a decay of the 2333 cm^{-1} band can be excluded because the observed SEIRA signals of CB[6] remain constant at potentials that already afford a significant decrease of the CB[6]•CO_2 band (Fig. 6c). This observation suggests that the effects of CB[6] host-guest chemistry can be exploited for CO_2 reduction at least at the desirable low overpotential region between –0.4 V and –0.7 V *vs.* RHE. Furthermore, it implies that part of the remaining surface-bound CB[6] has an empty cavity at potentials more negative than –0.8 V *vs*. RHE.

Plotting the 2343 cm^{-1} band observed on unmodified Au surfaces and in the presence of CB[6] yielded matching trends suggesting that CO_2 reduction of 'free' CO_2 proceeds in both cases in a similar environment (Fig. S13). A potential shift of the 2333 cm^{-1} absorption by around 40 mV at potential values affording turnover was noted, which may be related to an altered CO_2 reduction reaction within the cavity. CB[6]-bound CO was not detected as expected from the low binding affinity and solubility of CO. Moreover, CB[6] marker bands in CO_2-purged electrolyte were found to match those in Ar-purged solutions (Fig. S14) also at very negative potentials. This indicates that the structure and conformation of CB[6] is maintained throughout the large potential window and under CO_2 binding, suggesting that there is no change in CO_2 binding affinity particularly at negative potentials.

Electrocatalysis

Stepped constant potential electrolysis experiments were performed to monitor the influence of CB[6]•CO_2 on the activity and selectivity of CO_2 reduction on Au. The cell design with online gas sampling was based on recent reports,[69,70] and is described in detail in the Supporting Information (Fig. S15-17). Additional characterization including diffusion layer thickness and electrochemical surface area determination following a recent report for more standardized data acquisition[71] is also reported in the Supporting Information (Fig. S18-20). The system showed good stability for 12 h (Fig. S21). Fig. 7 compares partial current densities at various potentials of Au electrodes in solutions of CB[6] of varying concentrations to cover the CB[6] monolayer and multilayer regimes.

The results of unmodified (blank) Au agree with recently published results.[7] Self-assembly of CB[6] prior to catalysis without CB[6] in the electrolyte solution during electrocatalysis showed marginal differences compared to unfunctionalized Au electrodes (Fig. S22), which is presumably due to a less favorable adsorption equilibrium of CB[6] at negative applied potentials over the timespan of the electrocatalysis experiments.

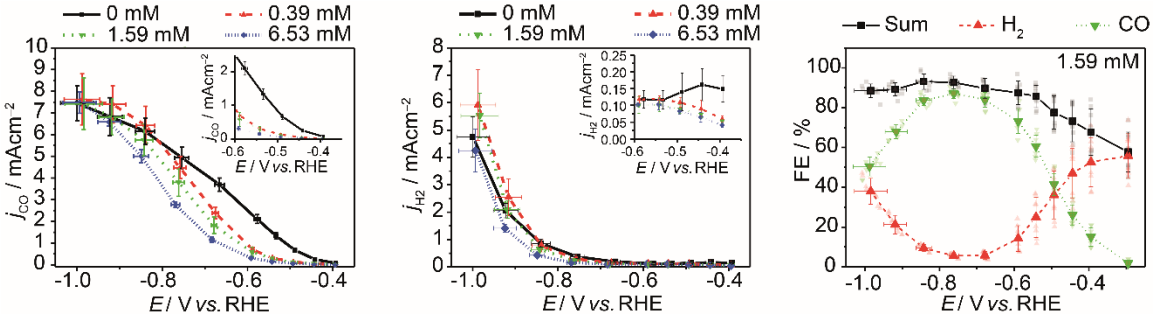

Fig. 7. Constant-potential electrolysis at seven potentials with online gas quantification. Data represents averages and standard deviations of at least three independent stepped-chronoamperometry experiments. X-axis error is calculated based on ±3 Ω change in uncompensated resistance. (a) partial CO current density (j_{CO}), (b) partial H_2 current density (j_{H2}) , (c) Faradaic efficiency of 1.59 mM CB[6] measurements.

In contrast, the presence of CB[6] in solution was found to selectively alter the CO partial current density (j_{CO}), while the hydrogen evolution current (j_{H2}) remained almost unchanged (Fig. 7). In the potential window from –0.4 V to –0.8 V *vs.* RHE, j_{CO} curves were observed to shift to more negative potentials with increasing CB[6] concentrations, corresponding to a suppression of j_{CO} with CB[6] in solution (Fig. 7a, further details of electrocatalysis data in Fig. S23-27). At 0.39 mM CB[6], an approximately 100 mV more negative potential was required to achieve a comparable j_{CO} than in the absence of CB[6]. No signals of CB[6] degradation were observed by nuclear magnetic resonance (NMR) spectroscopy (Fig. S28), and $^{13}CO_2$ electrocatalysis experiments yielded exclusively ^{13}CO (Fig. S29). Upon decreasing the potential more negative than –0.8 V *vs.* RHE, a convergence of the CO partial current densities in the absence and presence of CB[6] with different concentrations was observed (Fig. 7a). This observation can be rationalized by the potential-induced desorption of CB[6] from the surface starting to occur at potentials more negative than –0.7 V *vs.* RHE (Fig. 6c).

Mechanistic Interpretation

The experimental data demonstrate that the electrocatalytic reduction of CO_2 on Au has been effectively altered by CB[6] encapsulation. This effect can be explained on a molecular basis through the macrocycle's impact, particularly, on the rate determining step (RDS) of the catalytic process. In this respect, an initial electron transfer to CO_2 to form a Au-COO^- species or a proton coupled electron transfer to form directly a Au-COOH species are often discussed as possible candidates.[4,64,72–74] Both cases would yield a Tafel slope of 118 mV dec^{-1} based on the initial electron transfer as rate limiting step, which matches our Tafel slopes of approximately 120 mV dec^{-1} for unmodified and CB[6]-coated Au surfaces (Fig. S30). Thus, the unaffected Tafel slopes by the presence of CB[6] as well as the fact that only CO is generated allows to draw the conclusion that the macrocycle-mediated catalytic CO_2 reduction likely proceeds *via* the same elementary steps as on bare Au. The altered catalytic performance however suggests that the new reaction environment induced by CB[6] has significantly altered the kinetics of relevant reaction steps. This can be rationalized by an altered energy landscape for the reaction through specific interactions on CO_2 and COO^- within CB[6] compared to blank Au interface. This is provided by the following qualitative arguments:

(1) The hydrophobic nature of the cavity lowers the availability of water molecules to stabilize surface-bound intermediates through hydrogen bond formation. Previous molecular dynamics simulations suggest about 3-4 water molecules in the cavity of solubilized CB[6] without a guest in aqueous environment.[75] In line with this report, our MD simulations show that an average of less than one (0.62) water molecule is present within the space defined by the CB[6] carbonyl oxygen rims when CO_2 or CO are adsorbed in the CB[6] cavity.

(2) Cations such as K^+ have previously been shown to have a large effect on the CO_2 reduction reaction by stabilizing intermediates exhibiting a permanent dipole moment.[50] However, MD simulations show that the inclusion of K^+ into CB[6] is energetically unfavorable (Fig. S3), and DFT optimized structures of CB[6] with K^+ on a Au surface

suggest that the distance between K^+ and the surface bound intermediate COOH is too large for a stabilizing interaction (Fig. 8).

(3) Without further modifications, CB is known to stabilize electron deficient guests *via* hydrophobic interactions in the cavity and electrostatic interactions at the carbonyl rim. Hence, direct stabilization of a charged intermediate by the CB[6] cavity is likely not being provided.[26]

(4) DFT and MD calculations presented above revealed an approximatively 7 kcal mol^{-1} free energy difference of CO_2 in CB[6] compared to being freely diffusing in solution (Fig. 3 and Table S1). This indicates that CO_2 is stabilized within CB[6] and thus exhibits a reduced capability for subsequent reactions without additional stabilization of the reaction intermediate.

The altered environment within CB[6] will eventually affect the thermodynamics and kinetics of formation of encapsulated surface-bound species. To gauge such effects, DFT calculations were performed particularly for the Au-COOH species formation (details in the SI, Fig. S31-32). Calculations for Au-COO^- were not possible due the high level of complexity regarding the uncompensated charge. For CO_2, the results show a horizontally aligned molecule in the vicinity of the bare Au surface (Fig. S32), whereas a more perpendicular orientation was found within CB[6], suggesting that inclusion affords a different stabilization of the substrate near the electrode surface (Fig. 8).

Next, the reaction free energy difference ($\Delta\Delta_RG$) of the reaction from Au-CO_2 to Au-COOH within CB[6] and at the blank Au surface was calculated. An increase of ~8 kcal mol^{-1} (0.36 eV) was determined for the reaction proceeding in CB[6] compared to blank Au (Table S2). Thus, the calculation provides evidence for a notably increased energy required for the reaction upon encapsulation, which is proposed to result from the absence of solvent/cation-mediated stabilization of the product, *i.e.* Au-COOH as discussed qualitatively above, as well as from an additional stabilization of the substrate CO_2 within CB[6]. This effect is expected to be even more pronounced when considering Au-COO^- which should be energetically higher due to the absent charge compensation by the proton as well as the lack of other electrostatic interactions in the cavity as discussed above.

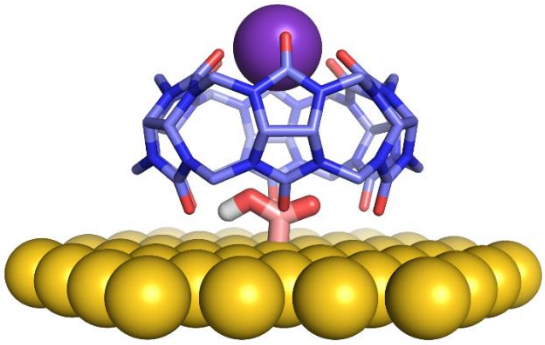

Fig. 8. DFT calculation-derived model of the Au-COOH intermediate in the CB[6] cavity on the Au surface. K^+ is coordinated to the carbonyl lined rim of CB[6]. Color coding: purple: K^+, red: O, yellow: Au, light blue: C (CB[6]), dark blue: N, white: H (not shown for CB[6] for increased clarity), light red: surface-bound C.

As a result, a higher-energy RDS is expected, leading to an overall decrease in j_{CO} (at the same applied potential) and therefore provides a molecular basis for explaining the increased overpotential required to reduce CO_2 inside the CB[6] cavity. In agreement, at 0.39 mM CB[6] concentration corresponding to a quasi-monolayer of CB[6] on Au, an indicative shift in j_{co} of the CB[6]-modified electrode by aforementioned ~100 mV was observed. In this context, increasing the CB[6] concentration to 1.59 mM CB[6] has little effect as the surface coverage is not significantly increased as demonstrated by QCM and SEIRA measurements (Fig. 5). However, at 6.53 mM CB[6], where multilayer formation occurs, a further, stronger suppression of the CO current density is apparent. Thus, for high CB[6] concentrations j_{CO} is likely governed by additional factors, such as hindered CO_2 uptake into CB[6] and CO release due to the adsorbed multilayers corresponding to an effective blocking of the electrode surface.

Host-guest design criteria for electrocatalysis

The rational manipulation of the heterogeneous interfacial catalytic process by creating well-defined reaction environments opens up promising avenues to selectively alter the catalytic transformation to desired outcomes in the future. Based on our findings, we

propose three design criteria to rationally achieve an improved molecular co-catalyst system for CO_2 reduction to CO:

(1) The induced reaction environment should be modulated to selectively stabilize the surface-bound intermediate COO^-/COOH to help break scaling relationships.[9] Recent publications discuss the ability of amines[76] and amides[18,19,77] in a ligand construct as well as imidazolium based ionic liquids[78,79] to stabilize CO_2 reduction intermediates *via* hydrogen bonding and/or electrostatic interactions on bare electrodes. In this respect, we envision that secondary guests within the CB cavity might be used to accommodate specific functional groups to selectively tune the active site environment. The larger CB[8] is able to incorporate two molecules within its cavity which offers a large degree of tunability of the electrostatic and chemical environment within the cavity.[26]

(2) The inclusion of the substrate CO_2 should facilitate consecutive reactions, for example, by enabling specific interactions of CO_2 with the cavity analogous to enzyme active sites. We observed a 10 cm^{-1} shift towards lower wavenumbers for CO_2 inside the CB[6] cavity. This may suggest a decreased bond order of CO_2. Nevertheless, this effect might not be dominant in the presented system due to the lack of stabilization of a key intermediate (COOH/COO^-). The probing of interactions of CO_2 with a secondary guest in the CB cavity *via* vibrational spectroscopy might enable systematic studies of host•substrate binding prior to catalytic turnover.

(3) The kinetics of CO_2 uptake and CO release need to be sufficiently fast to accomplish high catalytic activities. A simple model calculation (see SI) suggests that ingress and egress kinetics of CO_2 and CO, respectively, should be higher than 20 s^{-1} to obtain > 5 $mAcm^{-2}$ for j_{CO}. A high binding constant for CO_2 and low binding constant for CO should be maintained. The binding constant is defined as the ratio of ingress and egress kinetics,[46] and the egress kinetics for CO_2 and the ingress kinetics for CO should therefore be slow. While enzymes have perfected this independent tuning of complexation kinetics and thermodynamics, it remains difficult to realize this in synthetic systems. The use of cations as ‘lids’ for the CB-portals has been suggested to influence host-guest complex formation kinetics.[45] This might enable a pathway through variation of cations in the electrolyte solution to specifically alter the kinetics of substrate inclusion

or product release. Moreover, addition of competitively binding non-redox active guests could allow for further rationally tuning of CO_2 ingress/egress kinetics by subtly changing the host-guest-equilibria as well as electronics and sterics.

The manifold of new pathways to pursue shows that the CB[*n*]-Au hybrid system provides us with proposed measures and a modular platform to selectively tune different reaction steps of the heterogeneous CO_2 reduction at Au surfaces and to mechanistically explore electrocatalysis at the inorganic-organic interfaces. This allows for detailed investigations of the reaction mechanism by rational experimental design towards a complete understanding of the process. Such knowledge is a major prerequisite for the development of the next class of electrocatalysts with potential for real-world applications.

Conclusions

We present the concept of surface-adsorbed supramolecular host-guest chemistry in heterogeneous electrocatalysis. The combined spectroscopic, analytical and electrocatalytic results suggest that CO_2 is captured within the cavity of the supramolecular host-molecule CB[6] and is electrocatalytically reduced inside the cavity when adsorbed on the gold surface. An increased concentration of CO_2 is observed at the electrode-electrolyte interface due to the binding of CB[6]•CO_2.

The confinement of CO_2 reduction into CB[6] nanocavities enables molecular tunablity of the local chemical environment on the electrocatalyst surface. The presented data indicates that the CB[6]-complexation strongly and selectively affects the electrocatalytic reduction of CO_2 to CO, while the hydrogen evolution activity remains essentially unchanged. The resultant hybrid organic-inorganic composite can thus be regarded as a model system for synthetic cavity-based heterogeneous electrocatalysts. Notably, a plethora of different research fields spanning from metal-organic-frameworks[80,81] and covalent-organic-frameworks[82] to molecular catalysis[83–86] and synthetic biology[87] are also heavily focused on tuning the local environment and coordination spheres around a catalytic active site. The development of such model systems and analytical methodology as presented here may help to gain insight in this complex and important field of research. In the context of CO_2 reduction electrocatalysis,

this may offer new routes to overcome scaling relationships and rationally tune the selectivity and activity heterogeneous electrodes also beyond Au. Thus, this concept bridges the gap between enzymatic, molecular and heterogeneous catalysis and may open up new avenues for utilizing fine-tuned supramolecular units as synthetic catalytic pockets.

Supporting Information Detailed experimental procedures, additional transmission FTIR, SEIRA, QCM, XPS, MD, DFT, fluorescence, electrochemical characterization and electrocatalysis results.

Acknowledgement

We gratefully acknowledge financial support by the Christian Doppler Research Association, the Austrian Federal Ministry for Digital and Economic Affairs, the National Foundation for Research, Technology and Development, the OMV Group (to A.W., M.F.K., Er.R.), an EU ERC Consolidator grant 'MatEnSAP' (68283 to N.H., Er.R.) and Starting Grant 'BioNet' (757850 to Ed.R.), a Royal Society Newton International Fellowship (NF160054 to N.K.), European Commission for Marie Curie Fellowships (NANOSPHERE, 658360 to S.J.B.; VSHER, 701192 to K.H.L.; ESTIMABLeNANO, 706425 to K.S.), the EPSRC (EP/R013012/1 and EP/N020669/1 to Ed.R. and EP/L027151/1 for O.A.S.) and the DFG, Deutsche Forschungsgemeinschaft/German Research Foundation, (to K.I.A. and W.M.N.) as well as for funding under Germany´s Excellence Strategy – EXC 2008/1 (UniSysCat) – 390540038, (i.a. to I.Z.). We are also grateful to the UK Materials and Molecular Modelling Hub for computational resources, which is partially funded by EPSRC (EP/P020194/1). We would like to thank Mr. Simon Dowe for the help in the design and manufacturing of the electrochemical cell, Dr Guanglu Wu and Dr Annika Eisenschmidt for their help with NMR spectroscopy, Dr Jade Alexis McCune for a CB[6] sample and Mr. Dénes Berta for discussions regarding DFT computations.

References

(1) Qiao, J.; Liu, Y.; Hong, F.; Zhang, J. A Review of Catalysts for the

Electroreduction of Carbon Dioxide to Produce Low-Carbon Fuels. *Chem. Soc. Rev.* **2014**, *43*, 631–675.

(2) Lewis, N. S.; Nocera, D. G. Powering the Planet: Chemical Challenges in Solar Energy Utilization. *Proc. Natl. Acad. Sci.* **2006**, *103*, 15729–15735.

(3) Whipple, D. T.; Kenis, P. J. A. Prospects of CO_2 Utilization via Direct Heterogeneous Electrochemical Reduction. *J. Phys. Chem. Lett.* **2010**, *1*, 3451–3458.

(4) Kortlever, R.; Shen, J.; Schouten, K. J. P.; Calle-Vallejo, F.; Koper, M. T. M. Catalysts and Reaction Pathways for the Electrochemical Reduction of Carbon Dioxide. *J. Phys. Chem. Lett.* **2015**, *6*, 4073–4082.

(5) Jhong, H.-R. "Molly"; Ma, S.; Kenis, P. J. Electrochemical Conversion of CO_2 to Useful Chemicals: Current Status, Remaining Challenges, and Future Opportunities. *Curr. Opin. Chem. Eng.* **2013**, *2*, 191–199.

(6) Hori, Y.; Murata, A.; Kikuchi, K.; Suzuki, S. Electrochemical Reduction of Carbon Dioxides to Carbon Monoxide at a Gold Electrode in Aqueous Potassium Hydrogen Carbonate. *J. Chem. Soc. Chem. Commun.* **1987**, No. 10, 728.

(7) Cave, E. R.; Montoya, J. H.; Kuhl, K. P.; Abram, D. N.; Hatsukade, T.; Shi, C.; Hahn, C.; Nørskov, J. K.; Jaramillo, T. F. Electrochemical CO_2 Reduction on Au Surfaces: Mechanistic Aspects Regarding the Formation of Major and Minor Products. *Phys. Chem. Chem. Phys.* **2017**, *19*, 15856–15863.

(8) Chen, Y.; Li, C. W.; Kanan, M. W. Aqueous CO_2 Reduction at Very Low Overpotential on Oxide-Derived Au Nanoparticles. *J. Am. Chem. Soc.* **2012**, *134*, 19969–19972.

(9) Hansen, H. A.; Varley, J. B.; Peterson, A. A.; Nørskov, J. K. Understanding Trends in the Electrocatalytic Activity of Metals and Enzymes for CO_2 Reduction to CO. *J. Phys. Chem. Lett.* **2013**, *4*, 388–392.

(10) Zhu, W.; Zhang, Y.-J.; Zhang, H.; Lv, H.; Li, Q.; Michalsky, R.; Peterson, A. A.; Sun, S. Active and Selective Conversion of CO 2 to CO on Ultrathin Au Nanowires. *J. Am. Chem. Soc.* **2014**, *136*, 16132–16135.

(11) Shi, C.; Hansen, H. a; Lausche, A. C.; Nørskov, J. K. Trends in Electrochemical CO_2 Reduction Activity for Open and Close-Packed Metal Surfaces. *Phys. Chem. Chem. Phys.* **2014**, *16*, 4720.

(12) Li, Y.; Sun, Q. Recent Advances in Breaking Scaling Relations for Effective Electrochemical Conversion of CO_2. *Adv. Energy Mater.* **2016**, *6*, 1600463.

(13) Kim, D.; Resasco, J.; Yu, Y.; Asiri, A. M.; Yang, P. Synergistic Geometric and

Electronic Effects for Electrochemical Reduction of Carbon Dioxide Using Gold-Copper Bimetallic Nanoparticles. *Nat. Commun.* **2014**, *5*, 4948.

(14) Torelli, D. A.; Francis, S. A.; Crompton, J. C.; Javier, A.; Thompson, J. R.; Brunschwig, B. S.; Soriaga, M. P.; Lewis, N. S. Nickel–Gallium-Catalyzed Electrochemical Reduction of CO_2 to Highly Reduced Products at Low Overpotentials. *ACS Catal.* **2016**, *6*, 2100–2104.

(15) Calle-Vallejo, F.; Loffreda, D.; Koper, M. T. M.; Sautet, P. Introducing Structural Sensitivity into Adsorption–Energy Scaling Relations by Means of Coordination Numbers. *Nat. Chem.* **2015**, *7*, 403–410.

(16) Fang, Y.; Flake, J. C. Electrochemical Reduction of CO2 at Functionalized Au Electrodes. *J. Am. Chem. Soc.* **2017**, *139*, 3399–3405.

(17) Xie, M. S.; Xia, B. Y.; Li, Y.; Yan, Y.; Yang, Y.; Sun, Q.; Chan, S. H.; Fisher, A.; Wang, X. Amino Acid Modified Copper Electrodes for the Enhanced Selective Electroreduction of Carbon Dioxide towards Hydrocarbons. *Energy Environ. Sci.* **2016**, *9*, 1687–1695.

(18) Gong, M.; Cao, Z.; Liu, W.; Nichols, E. M.; Smith, P. T.; Derrick, J. S.; Liu, Y.-S.; Liu, J.; Wen, X.; Chang, C. J. Supramolecular Porphyrin Cages Assembled at Molecular–Materials Interfaces for Electrocatalytic CO Reduction. *ACS Cent. Sci.* **2017**, *3*, 1032–1040.

(19) Cao, Z.; Zacate, S. B.; Sun, X.; Liu, J.; Hale, E. M.; Carson, W. P.; Tyndall, S. B.; Xu, J.; Liu, X.; Liu, X.; Song, C.; Luo, J.; Cheng, M.-J.; Wen, X.; Liu, W. Tuning Gold Nanoparticles with Chelating Ligands for Highly Efficient Electrocatalytic CO_2 Reduction. *Angew. Chemie Int. Ed.* **2018**, *57*, 12675–12679.

(20) Cao, Z.; Kim, D.; Hong, D.; Yu, Y.; Xu, J.; Lin, S.; Wen, X.; Nichols, E. M.; Jeong, K.; Reimer, J. A.; Yang, P.; Chang, C. J. A Molecular Surface Functionalization Approach to Tuning Nanoparticle Electrocatalysts for Carbon Dioxide Reduction. *J. Am. Chem. Soc.* **2016**, *138*, 8120–8125.

(21) Shin, W.; Lee, S. H.; Shin, J. W.; Lee, S. P.; Kim, Y. Highly Selective Electrocatalytic Conversion of CO_2 to CO at −0.57 V (NHE) by Carbon Monoxide Dehydrogenase from Moorella t Hermoacetica. *J. Am. Chem. Soc.* **2003**, *125*, 14688–14689.

(22) Parkin, A.; Seravalli, J.; Vincent, K. A.; Ragsdale, S. W.; Armstrong, F. A. Rapid and Efficient Electrocatalytic CO_2/CO Interconversions by Carboxydothermus Hydrogenoformans CO Dehydrogenase I on an Electrode. *J. Am. Chem. Soc.* **2007**, *129*, 10328–10329.

(23) Robinson, W. E.; Bassegoda, A.; Reisner, E.; Hirst, J. Oxidation-State-Dependent Binding Properties of the Active Site in a Mo-Containing Formate Dehydrogenase.

J. Am. Chem. Soc. **2017**, *139*, 9927–9936.

(24) Shi, J.; Jiang, Y.; Jiang, Z.; Wang, X.; Wang, X.; Zhang, S.; Han, P.; Yang, C. Enzymatic Conversion of Carbon Dioxide. *Chem. Soc. Rev.* **2015**, *44*, 5981–6000.

(25) Can, M.; Armstrong, F. A.; Ragsdale, S. W. Structure, Function, and Mechanism of the Nickel Metalloenzymes, CO Dehydrogenase, and Acetyl-CoA Synthase. *Chem. Rev.* **2014**, *114*, 4149–4174.

(26) Barrow, S. J.; Kasera, S.; Rowland, M. J.; del Barrio, J.; Scherman, O. A. Cucurbituril-Based Molecular Recognition. *Chem. Rev.* **2015**, *115*, 12320–12406.

(27) You, H.; Wu, D.; Chen, Z.; Sun, F.; Zhang, H.; Chen, Z.; Cao, M.; Zhuang, W.; Cao, R. Highly Active and Stable Water Splitting in Acidic Media Using a Bifunctional Iridium/Cucurbit[6]Uril Catalyst. *ACS Energy Lett.* **2019**, *4*, 1301–1307.

(28) Kaifer, A. E. Toward Reversible Control of Cucurbit[*n*]Uril Complexes. *Acc. Chem. Res.* **2014**, *47*, 2160–2167.

(29) Mitkina, T. V.; Zakharchuk, N. F.; Naumov, D. Y.; Gerasko, O. A.; Fenske, D.; Fedin, V. P. Syntheses, Structures, and Electrochemical Properties of Inclusion Compounds of Cucurbit[8]Uril with Cobalt(III) and Nickel(II) Complexes. *Inorg. Chem.* **2008**, *47*, 6748–6755.

(30) Assaf, K. I.; Nau, W. M. Cucurbiturils: From Synthesis to High-Affinity Binding and Catalysis. *Chem. Soc. Rev.* **2015**, *44*, 394–418.

(31) Florea, M.; Nau, W. M. Strong Binding of Hydrocarbons to Cucurbituril Probed by Fluorescent Dye Displacement: A Supramolecular Gas-Sensing Ensemble. *Angew. Chemie Int. Ed.* **2011**, *50*, 9338–9342.

(32) An, Q.; Li, G.; Tao, C.; Li, Y.; Wu, Y.; Zhang, W. A General and Efficient Method to Form Self-Assembled Cucurbit[*n*]Uril Monolayers on Gold Surfaces. *Chem. Commun.* **2008**, *36*, 1989.

(33) Shin, J. W.; Bertocci, U.; Stafford, G. R. Stress Response to Surface Alloying and Dealloying during Underpotential Deposition of Pb on (111)-Textured Au. *J. Phys. Chem. C* **2010**, *114*, 7926–7932.

(34) Rojas, M. T.; Kaifer, A. E.; Königer, R.; Stoddart, J. F. Supported Monolayers Containing Preformed Binding Sites. Synthesis and Interfacial Binding Properties of a Thiolated β-Cyclodextrin Derivative. *J. Am. Chem. Soc.* **1995**, *117*, 336–343.

(35) Yao, Y.; Xue, M.; Zhang, Z.; Zhang, M.; Wang, Y.; Huang, F. Gold Nanoparticles Stabilized by an Amphiphilic Pillar[5]Arene: Preparation, Self-Assembly into Composite Microtubes in Water and Application in Green Catalysis. *Chem. Sci.*

2013, *4*, 3667.

(36) Kim, H.; Kim, Y.; Yoon, M.; Lim, S.; Park, S. M.; Seo, G.; Kim, K. Highly Selective Carbon Dioxide Sorption in an Organic Molecular Porous Material. *J. Am. Chem. Soc.* **2010**, *132*, 12200–12202.

(37) Mohan, M.; Suzuki, T.; Nair, A. K.; Pillai, S.; Warrier, K. G. K.; Hareesh, U. S.; Nair, B. N.; Gale, J. D. Surface Modification Induced Enhanced CO_2 Sorption in Cucurbit[6]Uril, an Organic Porous Material. *Phys. Chem. Chem. Phys.* **2017**, *19*, 25564–25573.

(38) Falk, M.; Miller, A. G. Infrared Spectrum of Carbon Dioxide in Aqueous Solution. *Vib. Spectrosc.* **1992**, *4*, 105–108.

(39) Mock, W. L.; Shih, N. Y. Structure and Selectivity in Host-Guest Complexes of Cucurbituril. *J. Org. Chem.* **1986**, *51*, 4440–4446.

(40) Pan, S.; Saha, R.; Mandal, S.; Mondal, S.; Gupta, A.; Fernández-Herrera, M. A.; Merino, G.; Chattaraj, P. K. Selectivity in Gas Adsorption by Molecular Cucurbit[6]Uril. *J. Phys. Chem. C* **2016**, *120*, 13911–13921.

(41) Ghale, G.; Nau, W. M. Dynamically Analyte-Responsive Macrocyclic Host–Fluorophore Systems. *Acc. Chem. Res.* **2014**, *47*, 2150–2159.

(42) Palma, A.; Artelsmair, M.; Wu, G.; Lu, X.; Barrow, S. J.; Uddin, N.; Rosta, E.; Masson, E.; Scherman, O. A. Cucurbit[7]Uril as a Supramolecular Artificial Enzyme for Diels-Alder Reactions. *Angew. Chemie Int. Ed.* **2017**, *56*, 15688–15692.

(43) Lee, T.-C.; Scherman, O. A. Formation of Dynamic Aggregates in Water by Cucurbit[5]Uril Capped with Gold Nanoparticles. *Chem. Commun.* **2010**, *46*, 2438.

(44) McCune, J. A.; Kunz, S.; Olesińska, M.; Scherman, O. A. DESolution of CD and CB Macrocycles. *Chem. Eur. J.* **2017**, *23*, 8601–8604.

(45) Jeon, Y.-M.; Kim, J.; Whang, D.; Kim, K. Molecular Container Assembly Capable of Controlling Binding and Release of Its Guest Molecules: Reversible Encapsulation of Organic Molecules in Sodium Ion Complexed Cucurbituril. *J. Am. Chem. Soc.* **1996**, *118*, 9790–9791.

(46) Márquez, C.; Hudgins, R. R.; Nau, W. M. Mechanism of Host−Guest Complexation by Cucurbituril. *J. Am. Chem. Soc.* **2004**, *126*, 5806–5816.

(47) Murata, A.; Hori, Y. Product Selectivity Affected by Cationic Species in Electrochemical Reduction of CO 2 and CO at a Cu Electrode. *Bull. Chem. Soc. Jpn.* **1991**, *64*, 123–127.

(48) Kyriacou, G. Z.; Anagnostopoulos, A. K. Influence CO_2 Partial Pressure and the Supporting Electrolyte Cation on the Product Distribution in CO_2 Electroreduction. *J. Appl. Electrochem.* **1993**, *23*, 483–486.

(49) Thorson, M. R.; Siil, K. I.; Kenis, P. J. a. Effect of Cations on the Electrochemical Conversion of CO_2 to CO. *J. Electrochem. Soc.* **2012**, *160*, F69–F74.

(50) Resasco, J.; Chen, L. D.; Clark, E.; Tsai, C.; Hahn, C.; Jaramillo, T. F.; Chan, K.; Bell, A. T. Promoter Effects of Alkali Metal Cations on the Electrochemical Reduction of Carbon Dioxide. *J. Am. Chem. Soc.* **2017**, *139*, 11277–11287.

(51) Kuhl, K. P.; Hatsukade, T.; Cave, E. R.; Abram, D. N.; Kibsgaard, J.; Jaramillo, T. F. Electrocatalytic Conversion of Carbon Dioxide to Methane and Methanol on Transition Metal Surfaces. *J. Am. Chem. Soc.* **2014**, *136*, 14107–14113.

(52) Kim, D.; Kley, C. S.; Li, Y.; Yang, P. Copper Nanoparticle Ensembles for Selective Electroreduction of CO_2 to C_2 –C_3 Products. *Proc. Natl. Acad. Sci.* **2017**, *114*, 10560–10565.

(53) Sauerbrey, G. Verwendung von Schwingquarzen Zur Waegung Duenner Schichten Und Zur Mikrowaegung. *Zeitschrift fuer Phys.* **1959**, *155*, 206–222.

(54) Singh, K.; Blanford, C. F. Electrochemical Quartz Crystal Microbalance with Dissipation Monitoring: A Technique to Optimize Enzyme Use in Bioelectrocatalysis. *ChemCatChem* **2014**, *6*, 921–929.

(55) Dixon, M. C. Quartz Crystal Microbalance with Dissipation Monitoring: Enabling Real-Time Characterization of Biological Materials and Their Interactions. *J. Biomol. Tech.* **2008**, *19*, 151–158.

(56) Notley, S. M.; Eriksson, M.; Wågberg, L. Visco-Elastic and Adhesive Properties of Adsorbed Polyelectrolyte Multilayers Determined in Situ with QCM-D and AFM Measurements. *J. Colloid Interface Sci.* **2005**, *292*, 29–37.

(57) Blanco, E.; Quintana, C.; Hernández, L.; Hernández, P. Atomic Force Microscopy Study of New Sensing Platforms: Cucurbit[*n*]Uril (*n* =6, 7) on Gold. *Electroanalysis* **2013**, *25*, 263–268.

(58) Heo, J.; Kim, J.; Whang, D.; Kim, K. Columnar One-Dimensional Coordination Polymer Formed with a Metal Ion and a Host–Guest Complex as Building Blocks: Potassium Ion Complexed Cucurbituril. *Inorganica Chim. Acta* **2000**, *297*, 307–312.

(59) Ni, X.-L.; Xiao, X.; Cong, H.; Liang, L.-L.; Cheng, K.; Cheng, X.-J.; Ji, N.-N.; Zhu, Q.-J.; Xue, S.-F.; Tao, Z. Cucurbit[n]Uril-Based Coordination Chemistry: From Simple Coordination Complexes to Novel Poly-Dimensional Coordination Polymers. *Chem. Soc. Rev.* **2013**, *42*, 9480.

(60) Osawa, M.; Ataka, K.; Ikeda, M.; Uchihara, H.; Nanba, R. Surface Enhanced Infrared Absorption Spectroscopy. *Anal. Sci.* **1991**, *7*, 503–506.

(61) Wisitruangsakul, N.; Zebger, I.; Ly, K. H.; Murgida, D. H.; Ekgasit, S.; Hildebrandt, P. Redox-Linked Protein Dynamics of Cytochrome c Probed by Time-Resolved Surface Enhanced Infrared Absorption Spectroscopy. *Phys. Chem. Chem. Phys.* **2008**, *10*, 5276.

(62) Chikkaraddy, R.; de Nijs, B.; Benz, F.; Barrow, S. J.; Scherman, O. A.; Rosta, E.; Demetriadou, A.; Fox, P.; Hess, O.; Baumberg, J. J. Single-Molecule Strong Coupling at Room Temperature in Plasmonic Nanocavities. *Nature* **2016**, *535*, 127–130.

(63) Osawa, M. Surface-Enhanced Infrared Absorption. In *Near-Field Optics and Surface Plasmon Polaritons*; Springer Berlin Heidelberg: Berlin, Heidelberg, 2001; pp 163–187.

(64) Wuttig, A.; Yaguchi, M.; Motobayashi, K.; Osawa, M.; Surendranath, Y. Inhibited Proton Transfer Enhances Au-Catalyzed CO_2-to-Fuels Selectivity. *Proc. Natl. Acad. Sci.* **2016**, *113*, E4585–E4593.

(65) Wuttig, A.; Liu, C.; Peng, Q.; Yaguchi, M.; Hendon, C. H.; Motobayashi, K.; Ye, S.; Osawa, M.; Surendranath, Y. Tracking a Common Surface-Bound Intermediate during CO_2-to-Fuels Catalysis. *ACS Cent. Sci.* **2016**, *2*, 522–528.

(66) Dunwell, M.; Lu, Q.; Heyes, J. M.; Rosen, J.; Chen, J. G.; Yan, Y.; Jiao, F.; Xu, B. The Central Role of Bicarbonate in the Electrochemical Reduction of Carbon Dioxide on Gold. *J. Am. Chem. Soc.* **2017**, *139*, 3774–3783.

(67) Heidary, N.; Ly, K. H.; Kornienko, N. Probing CO2 Conversion Chemistry on Nanostructured Surfaces with Operando Vibrational Spectroscopy. *Nano Lett.* **2019**, *19*, 4817–4826.

(68) Love, J. C.; Estroff, L. a.; Kriebel, J. K.; Nuzzo, R. G.; Whitesides, G. M. Self-Assembled Monolayers of Thiolates on Metals as a Form of Nanotechnology. *Chem. Rev.* **2005**, *105*, 1103–1170.

(69) Kuhl, K. P.; Cave, E. R.; Abram, D. N.; Jaramillo, T. F. New Insights into the Electrochemical Reduction of Carbon Dioxide on Metallic Copper Surfaces. *Energy Environ. Sci.* **2012**, *5*, 7050.

(70) Lobaccaro, P.; Singh, M. R.; Clark, E. L.; Kwon, Y.; Bell, A. T.; Ager, J. W. Effects of Temperature and Gas–Liquid Mass Transfer on the Operation of Small Electrochemical Cells for the Quantitative Evaluation of CO_2 Reduction Electrocatalysts. *Phys. Chem. Chem. Phys.* **2016**, *18*, 26777–26785.

(71) Clark, E. L.; Resasco, J.; Landers, A.; Lin, J.; Chung, L.-T.; Walton, A.; Hahn, C.;

Jaramillo, T. F.; Bell, A. T. Standards and Protocols for Data Acquisition and Reporting for Studies of the Electrochemical Reduction of Carbon Dioxide. *ACS Catal.* **2018**, *8*, 6560–6570.

(72) Wuttig, A.; Yoon, Y.; Ryu, J.; Surendranath, Y. Bicarbonate Is Not a General Acid in Au-Catalyzed CO_2 Electroreduction. *J. Am. Chem. Soc.* **2017**, *139*, 17109–17113.

(73) Dunwell, M.; Luc, W.; Yan, Y.; Jiao, F.; Xu, B. Understanding Surface-Mediated Electrochemical Reactions: CO_2 Reduction and Beyond. *ACS Catal.* **2018**, 8121–8129.

(74) Zhang, B. A.; Ozel, T.; Elias, J. S.; Costentin, C.; Nocera, D. G. Interplay of Homogeneous Reactions, Mass Transport, and Kinetics in Determining Selectivity of the Reduction of CO_2 on Gold Electrodes. *ACS Cent. Sci.* **2019**, *5*, 1097–1105.

(75) Biedermann, F.; Uzunova, V. D.; Scherman, O. A.; Nau, W. M.; De Simone, A. Release of High-Energy Water as an Essential Driving Force for the High-Affinity Binding of Cucurbit[n]Urils. *J. Am. Chem. Soc.* **2012**, *134*, 15318–15323.

(76) Azcarate, I.; Costentin, C.; Robert, M.; Savéant, J.-M. Through-Space Charge Interaction Substituent Effects in Molecular Catalysis Leading to the Design of the Most Efficient Catalyst of CO_2-to-CO Electrochemical Conversion. *J. Am. Chem. Soc.* **2016**, *138*, 16639–16644.

(77) Nichols, E. M.; Derrick, J. S.; Nistanaki, S. K.; Smith, P. T.; Chang, C. J. Positional Effects of Second-Sphere Amide Pendants on Electrochemical CO_2 Reduction Catalyzed by Iron Porphyrins. *Chem. Sci.* **2018**, *9*, 2952–2960.

(78) Rosen, B. a; Salehi-Khojin, A.; Thorson, M. R.; Zhu, W.; Whipple, D. T.; Kenis, P. J. a; Masel, R. I. Ionic Liquid-Mediated Selective Conversion of CO_2 to CO at Low Overpotentials. *Science (80-.).* **2011**, *334*, 643–644.

(79) Lau, G. P. S.; Schreier, M. R.; Vasilyev, D.; Scopelliti, R.; Grätzel, M.; Dyson, P. J. New Insights Into the Role of Imidazolium-Based Promoters for the Electroreduction of CO_2 on a Silver Electrode. *J. Am. Chem. Soc.* **2016**, jacs.6b03366.

(80) Hendon, C. H.; Rieth, A. J.; Korzyński, M. D.; Dincă, M. Grand Challenges and Future Opportunities for Metal-Organic Frameworks. *ACS Cent. Sci.* **2017**, *3*, 554–563.

(81) Hod, I.; Sampson, M. D.; Deria, P.; Kubiak, C. P.; Farha, O. K.; Hupp, J. T. Fe-Porphyrin-Based Metal–Organic Framework Films as High-Surface Concentration, Heterogeneous Catalysts for Electrochemical Reduction of CO 2. *ACS Catal.* **2015**, *5*, 6302–6309.

(82) Diercks, C. S.; Lin, S.; Kornienko, N.; Kapustin, E. A.; Nichols, E. M.; Zhu, C.; Zhao, Y.; Chang, C. J.; Yaghi, O. M. Reticular Electronic Tuning of Porphyrin Active Sites in Covalent Organic Frameworks for Electrocatalytic Carbon Dioxide Reduction. *J. Am. Chem. Soc.* **2018**, *140*, 1116–1122.

(83) Ginovska-Pangovska, B.; Dutta, A.; Reback, M. L.; Linehan, J. C.; Shaw, W. J. Beyond the Active Site: The Impact of the Outer Coordination Sphere on Electrocatalysts for Hydrogen Production and Oxidation. *Acc. Chem. Res.* **2014**, *47*, 2621–2630.

(84) Caserta, G.; Roy, S.; Atta, M.; Artero, V.; Fontecave, M. Artificial Hydrogenases: Biohybrid and Supramolecular Systems for Catalytic Hydrogen Production or Uptake. *Curr. Opin. Chem. Biol.* **2015**, *25*, 36–47.

(85) Reuillard, B.; Warnan, J.; Leung, J. J.; Wakerley, D. W.; Reisner, E. A Poly(Cobaloxime)/Carbon Nanotube Electrode: Freestanding Buckypaper with Polymer-Enhanced H_2-Evolution Performance. *Angew. Chemie Int. Ed.* **2016**, *55*, 3952–3957.

(86) Birdja, Y. Y.; Vos, R. E.; Wezendonk, T. A.; Jiang, L.; Kapteijn, F.; Koper, M. T. M. Effects of Substrate and Polymer Encapsulation on CO_2 Electroreduction by Immobilized Indium(III) Protoporphyrin. *ACS Catal.* **2018**, *8*, 4420–4428.

(87) Lancaster, L.; Abdallah, W.; Banta, S.; Wheeldon, I. Engineering Enzyme Microenvironments for Enhanced Biocatalysis. *Chem. Soc. Rev.* **2018**, *47*, 5177–5186.

Table of Contents Artwork: